Plasticity and fluctuations in quasi-two-dimensional hopper flow of emulsions

Dandan Chen,* Kenneth W. Desmond, and Eric R. Weeks
Department of Physics, Emory University, Atlanta, GA 30322
(Dated: May 17, 2011)

We experimentally study the shear flow of oil-in-water emulsion droplets in a thin sample chamber with a hopper shape. In this thin chamber, the droplets are formed into quasi-2D pancakes, somewhat analogous to soft photoelastic disks. From the deformations of the droplet outlines, we observe large stress fluctuations, similar to what has been seen in granular flow through hoppers. We show a direct and local relationship between T1 events (where four droplets rearrange, exchanging neighbors) and the macroscopic stress fluctuations. A T1 event influences the stress up to 3 droplet diameters away.

PACS numbers: 83.80.Iz, 47.50.Ef, 83.10.Bb

Simple fluids at low flow rates flow laminarly, with the flow field independent of time. In contrast, the flow of complex materials such as sand, foam, and emulsions exhibit strong fluctuations even at low flow rates [1–5]. This macroscopic observation is not surprising as microscopically the individual grains (or bubbles or droplets) in a material must rearrange to allow for flow [6], and their discrete size gives rise to measurable fluctuations in properties such as the macroscopic stress. Furthermore, the forces felt by individual particles vary quite widely in granular materials, with a small subset of particles bearing large forces [7–9]. The heterogeneity of forces has been seen also in experiments with emulsion droplets [10, 11], foams [12], and simulations of frictionless particles [13]. Much prior work has attempted to connect the microscopic (particle-scale) forces and rearrangements to the macroscopic stress fluctuations [1, 2, 14, 15]. Some theoretical work [15–18] and simulations [19] suggest a connection between individual microscopic plastic rearrangements and the local stress field. Recent work showed that the ability of local rearrangements to relax the stress within the surrounding region is important for understanding the flow properties of a complex fluid, although this work did not directly visualize the rearrangements [17, 18].

In this Letter, we use an experiment with quasi-two-dimensional emulsion droplets to study the relation between local structural changes and macroscopic stress fluctuations. Small oil droplets are compressed between two parallel glass plates, deforming them into disks similar to photoelastic disk experiments [8, 9] or some quasi-two-dimensional foams [12, 15, 19]. The sample is jammed, and the stress each droplet feels is quantified by examining each droplet's deviation from a circular shape. In particular, we study T1 events, where four droplets exchange neighbors, as shown in Fig. 1(a-c) [2, 3, 6, 15, 19]. These rearrangements are induced by flowing the sample through a hopper [Fig. 1(d)] [4, 14, 20]. We find that T1 events diminish the stresses felt by droplets over a distance up to ~ 3 diameters away from the event, and thus these local rearrangements have a nonlocal influence on the macroscopic stress.

Our droplets are silicon oil (poly-dimethylsiloxane, ρ=1 g/mL, η=350 mPas) in water, stabilized by Fairy^{TM} soap of mass fraction 0.025, and are produced with the "co-flow" microfluidic technique [21]. We place the droplets into quasi-two-dimensional hoppers shaped using a thin film of Scotch$^{\mathrm{TM}}$ tape with thickness 0.10±0.02 mm. The samples have area fractions $\phi \geq 0.90$ as shown in Table I. At these high area fractions, all of our samples are in the jammed state [3, 13]. At lower area fractions (less than the jamming point, $\phi_J \approx 0.84$), the surface tension ensures the droplets are perfectly round, but for our experiments at $\phi \geq 0.90$ all of the droplets are slightly deformed. The details for our six experimental runs are given in Table I. The standard deviation of the droplet radii is sufficiently large in all cases to frustrate long-range order. Our results depend only on the mean radius $\langle r \rangle$ as will be described below, and do not otherwise change with different size distributions.

Run	A	$\tilde{A}$	ϕ	$\langle r \rangle$	$\sigma/\langle r \rangle$	s	Θ
1	2.93	12.8	0.90	0.27	0.21	0.010	25
2	1.33	18.8	0.90	0.15	0.17	-0.009	25
3	0.83	5.5	0.92	0.22	0.27	-0.010	27
4	0.75	14.1	0.93	0.13	0.24	-0.007	27
5	0.61	9.9	0.91	0.14	0.21	-0.010	26
6	0.33	6.2	0.94	0.13	0.28	-0.002	27

TABLE I: Sample details of our six runs. The columns are flux rate A (mm^{2}s^{-1}), normalized flux rate $\tilde{A} = A/\pi\langle r \rangle^2$ (s^{-1}), area fraction ϕ, mean droplet radius $\langle r \rangle$ (mm), standard deviation $\sigma = \sqrt{\langle (r - \langle r \rangle)^2 \rangle}$ normalized by $\langle r \rangle$, skewness $s = \langle (\frac{r - \langle r \rangle}{\sigma})^3 \rangle$, and hopper angle Θ (degrees).

We image the droplets with a 1.6× objective on an inverted microscope, using a 30 frame/s camera and a 0.33× camera-mount. A constant flux rate is set by a syringe pump. Similar to the flow behavior of other jammed materials [3, 6, 8, 15, 17], we find the time-averaged flow is smooth despite the complex motions of the indi-

*Electronic address: dchen361@gmail.com

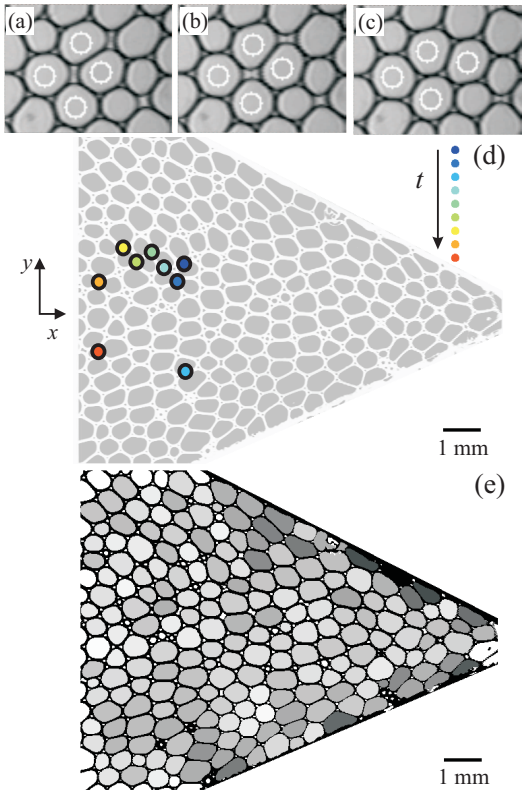

FIG. 1: (Color) (a)-(c) The three images show a typical T1 rearrangement of the four particles labeled by white circles. The field of view is 1.6×1.2 mm^2, and the time interval between consecutive images is 0.66 s. (d) Snapshot of sample. The flow direction is from left to right. The colored circles show the positions of T1 events taken from the time sequence of Fig. 3(b), where the earliest color (dark blue) corresponds to the T1 event at $t = 38.7$ s and the latest color (red) corresponds to the event at $t = 47.3$ s. Five of these T1 events occur in the time window $t = (44.5\text{ s}, 46.2\text{ s})$ during which the droplets in that region move downstream only 0.5 mm; these five events are the leftmost events of the top group shown in the image. The background image, taken at $t = 45.2$ s, has been inverted for better visualization. Each T1 event is positioned at the center of the four droplets comprising the T1 event based on their positions at $t = 45.2$ s. The data correspond to run 1 of Table I. (e) This image corresponds to (d), and is shaded based on the deformation D of each droplet. The darkest droplets correspond to $D = 0.4$ and white corresponds to $D = 0$.

vidual droplets. Our time-averaged velocity profiles are parabolic, described by

$$V_x(x, y) = \alpha(x) + \beta(x)y^2, \tag{1}$$

where $y = 0$ is the centerline of the channel, α is the flow rate along the centerline, and β relates to the local strain rate. Droplets at the side walls slip along the wall with the velocity of $V_x(x, \frac{w(x)}{2}) > 0$, where $w(x)$ is the channel width that droplet centers can reach. The parameters α and β are proportional to the flux rate A as

$$\alpha = \frac{k_\alpha A}{\big(w(x) + 2\langle r\rangle\big)}, \beta = \frac{-k_\beta A}{\big(w^3(x) + 6\langle r\rangle w^2(x)\big)}. \tag{2}$$

Equations 1 and 2, and parameters $k_\alpha = 1.24$ and $k_\beta = 2.87$ are all empirical observations. We find $V_y \sim 0.1V_x$ in all regions within the sample chamber. The equations above ensure that the flux rate A is independent of position x.

To quantify stress fluctuations in the flowing sample, we first examine the shapes of individual droplets to determine their stresses. Droplets are deformed away from perfect circles by forces from neighboring droplets [10, 11]. We quantify the deformation by determining the outline of each droplet, finding the radius r at each point on the outline (measured from the center of mass of the droplet), and then defining the droplet deformation as $D = \sqrt{\langle r^2\rangle - \langle r\rangle^2}/\langle r\rangle$, the standard deviation of r normalized by that droplet's mean radius.

Figure 1(e) shows the spatial distribution of D at one instant in time. D rises near the hopper exit, similar to jamming arches found in granular materials [4]. We find that the mean deformation obeys $\langle D\rangle_{y,t}(x) = D_0[1 + A/k_v w(x)]$, with fitting parameters $k_v = 0.81$ mm/s as a velocity scale and $D_0 = 0.06$ as the deformation for a non-flowing suspension at area fraction $\phi \approx 0.9$. In the absence of flow, $\langle D\rangle_y = D_0$; having $\langle D\rangle_y > D_0$ is because the nonzero flux rate results in droplets being deformed quicker than they can relax. This relaxation is limited by the viscosity. The deformation rises near the walls and near the constriction, where the local shear rates are highest. In most of our analysis below, we will focus on the left side of the sample chamber, where $w(x)$ is large and thus $\langle D\rangle_{y,t} \approx D_0$ is moderately independent of x.

By averaging the deformation of all droplets within a large region as a function of time, we measure the macroscopic stress changes, as shown in Fig. 2(a). These stress fluctuations are similar to those seen in granular hopper experiments [4, 14, 20]. In particular, the stress builds up and then can release during a short time interval, with the magnitude of the stress drop fairly significant ($|\Delta D_{drop}| > 0.2\langle D\rangle$). We plot the power spectra of the stress fluctuations for three different regions of the sample chamber in Fig. 2(b). At high frequencies the spectrum is consistent with a power law $P(\omega) \sim \omega^{-1}$. This is similar to various constant strain studies on the flow of granular materials, foams, and emulsions which found $P(\omega) \sim \omega^{-1}$ or $\sim \omega^{-2}$ [1, 14, 22–24].

These stress fluctuations are related to localized rearrangement events, such as the T1 event shown in Fig. 1(a-c). To illustrate this, in Fig. 3(a) we plot a short segment of the $D(t)$ data from Fig. 2(a). During this time period, we also count the number of T1 rearrangements that occur in the same region, and show the cumulative number in Fig. 3(b). Comparing these two figures shows that T1 events happen more frequently during periods of large stress drops (36-38 s and 45-46 s). Furthermore, these events are spatially correlated, as shown in Fig. 1(d),

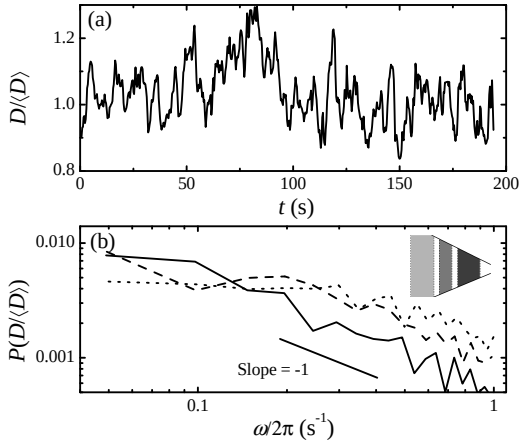

FIG. 2: (a) Temporal fluctuations of the mean deformation in the left part of hopper; this is the left-most shaded region in the inset of (b). This is from run 1 (Table I). (b) Power spectra of the deformation fluctuations at 3 different regions along the channel as shown in the inset. The boundaries of the regions are (0.3 mm, 3.4 mm) – solid line, (4.2 mm, 5.9 mm) – dashed line, and (6.6 mm, 9.6 mm) – dotted line. These regions contain $\sim$ 100, 50, and 50 droplets respectively. For this sample chamber, the width is $w(x) = 2(x_0 - x)\tan(\Theta)$ with $x_0 = 11.86$ mm and $\Theta = 25^\circ$.

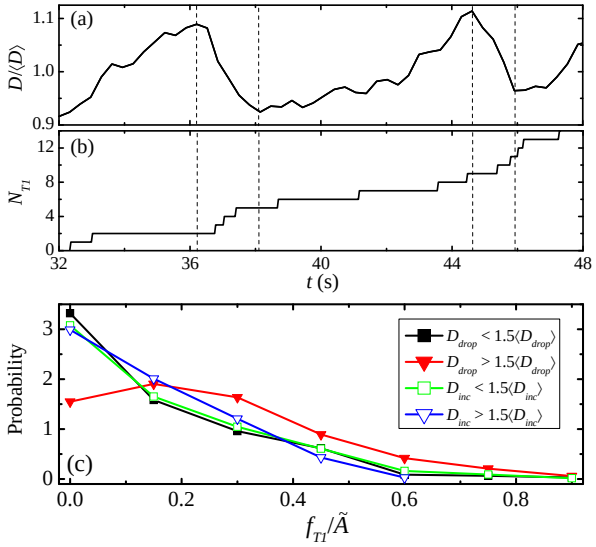

FIG. 3: (Color online) (a) Subset of data from Fig. 2(a), showing the fluctuations of the mean deformation within the left-most region of the sample chamber. (b) The cumulative number of T1 events in that region over the same period of time. The vertical dashed lines in (a) and (b) indicate the time intervals when the mean deformation significantly drops. (c) The probability distribution of the frequency of T1 events f_{T1} divided by the normalized flux rate $\tilde{A} = A/\pi\langle r\rangle^2$ for all six runs of Table I, with the different curves corresponding to different regimes for deformation changes, as indicated in the legend. Open symbols correspond to deformation increases, and closed symbols to deformation drops. The data correspond to the left-most regions of each channel, similar to the left region shown in the inset of Fig. 2(b).

which shows the locations of the T1 events occurring between 38 s and 48 s. Clearly one T1 event can trigger rearrangements of other nearby droplets [5].

Further evidence linking large deformation drops to groups of T1 events is found by calculating the frequency of T1 events f_{T1} during a deformation drop, defined by counting the number of T1 events occurring divided by the length of time over which the deformation changes monotonically. The probability distributions of f_{T1} are shown in Fig. 3(c) for different sized deformation changes. The inverted solid triangles are the distribution for the largest deformation drops, and this distribution is noticeably shifted to larger frequencies. These distributions collapse across data sets when f_{T1} is scaled by the normalized flux rate $\tilde{A} = A/\pi\langle r\rangle^2$, and so Fig. 3(c) shows data from all six runs put together in this fashion. Figure 3(c) is direct evidence that large stress relaxations are highly correlated with bursts of T1 events. Theoretical work suggests that the rate of rearrangements is a useful way to characterize the fluidity of jammed materials [18], and our observations show a connection between this fluidity and the large stress relaxations.

Given the correlation between T1 events and large stress drops (Fig. 3), we next consider how an individual T1 event influences the deformation of nearby droplets. We define $\Delta t = 0$ to be the instant of a T1 event [Fig. 1(b)]. Distances from the T1 event are measured by ΔR, where $\Delta R = 0$ is taken to be the center of the four droplets involved in the T1 event at the specific time Δt, that is, ΔR is measured in a co-moving reference frame. The mean deformation D as a function of ΔR is shown in Fig. 4(a) for several different Δt's both before and after the T1 event. Before the T1 event, the stress builds up primarily at $\Delta R < 2\langle r\rangle$, where $\langle r\rangle$ is the mean droplet radius; this stress buildup reflects strong deformation of the four droplets that will be involved in the T1 event. At the T1 event, the four droplets involved in the T1 event dramatically decrease their deformation [solid circles in Fig. 4(a)], and quickly this stress release is propagated outward to distances $\Delta R = 6\langle r\rangle$. This strong influence of the T1 event on the neighboring droplets confirms the prediction of previous simulations [4, 13, 19] and theories [16–18]. Our length scale ($\sim$ 3 droplets) matches an inferred dynamic length scale in a recent three-dimensional emulsion experiment ($\sim 3-4$ droplet diameters) [17]. Together with Fig. 1(d), the overall picture is that T1 events can cascade and release stress over a large region, leading to the fluctuations seen in Fig. 2(a).

A more detailed space-time plot of the deformation is shown in Fig. 4(b), where red indicates larger than average deformation, and blue indicates smaller than average deformation. This is the same data shown in Fig. 4(a). Again, it can be seen that the stress builds up before the T1 event and relaxes quickly afterward. At long times $\Delta t > 5$ s, the stress returns to its mean value. The structure of the space-time plot can be understood by looking at Fig. 4(c), which indicates the number of

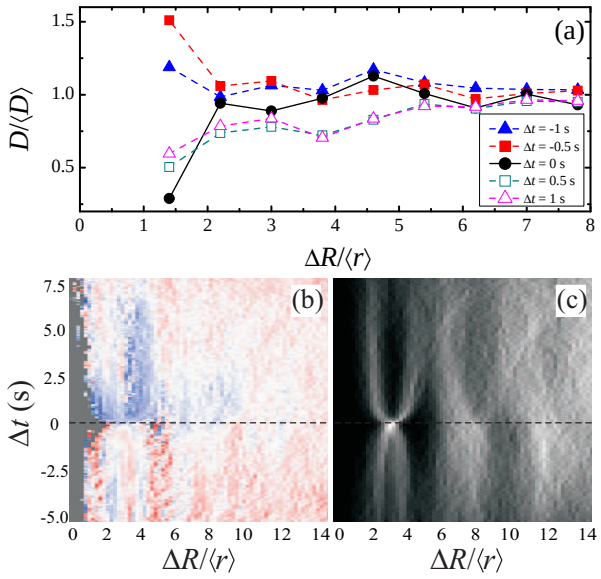

FIG. 4: (a) Mean deformation around a T1 event, averaging over 186 T1 events during a 194 s duration movie (run 1). These events all occur in the left side of the channel, see the inset to Fig. 2(b). The distance ΔR is defined in the frame of reference co-moving with the center of the four droplets undergoing the T1 rearrangement; for these data, this frame of reference moves roughly one mean radius per second. The T1 event occurs at $\Delta t = 0$ s. (b) Space-time plot of the same data with higher resolution. Red indicates deformation larger than the mean, white is the mean, and blue is deformation smaller than the mean. (c) Space-time plot showing where droplets are found, relative to the T1 event. White corresponds to the most probable positions of droplets. The stretched X-shape on the left side corresponds to the most probable positions of the four droplets undergoing the T1 event.

droplets found at a given $\Delta R, \Delta t$. The intense white regions are where droplets are found with high probability, and the "X" shape located at $2 < \Delta R/\langle r\rangle < 4$ corresponds to the four droplets involved with the T1 event. Two of these droplets start apart and come together, ending at $\Delta R \approx 2\langle r\rangle$, while the other two droplets initially are neighbors and then separate, ending at $\Delta R \approx 4\langle r\rangle$. These four droplets are the ones which most strongly change their deformation in Fig. 4(b).

We have used a quasi-two-dimensional emulsion to investigate the correlation between microscopic dynamics and macroscopic stresses in a dense flow through a hopper. Local rearrangements ("T1 events") occur in bursts and are correlated with large local stress releases; this is a direct connection between microscopic structural changes and macroscopically observable stress fluctuations. We observe a length scale for this correlation, where local T1 events result in stress releases influencing droplets as far as three droplet diameters away. Our results are for a system without static friction; it is intriguing that the stress fluctuations we see are similar to those seen in granular experiments [1, 8, 14, 20]. These similarities suggest that the connections we see between individual rearrangements, groups of these rearrangements, and macroscopic stress fluctuations, may be common characteristics of complex fluids under shear for both frictionless and frictional systems.

We thank S. Devaiah, A. Fernandez-Nieves, X. Hong, Y. Jiang, T. Lopez-Leon, M. L. Manning, N. Xu, and P. J. Young for helpful discussions. D. Chen, K. W. Desmond, and E. R. Weeks were supported by the donors of The Petroleum Research Fund, administered by the American Chemical Society. This material is also based upon work supported by the National Science Foundation under Grant No. CBET-0853837.

[1] B. Miller, C. O'Hern, and R. P. Behringer, Phys. Rev. Lett. **77**, 3110 (1996).
[2] M. Dennin, Phys. Rev. E **70**, 041406 (2004).
[3] J. Lauridsen, G. Chanan, and M. Dennin, Phys. Rev. Lett. **93**, 018303 (2004).
[4] S. Tewari, B. Tithi, A. Ferguson, and B. Chakraborty, Phys. Rev. E **79**, 011303 (2009).
[5] D. J. Durian, Phys. Rev. Lett. **75**, 4780 (1995).
[6] M. Dennin and C. M. Knobler, Phys. Rev. Lett. **78**, 2485 (1997).
[7] C. H. Liu, Phys. Rev. B **50**, 782 (1994).
[8] D. Howell, R. P. Behringer, and C. Veje, Phys. Rev. Lett. **82**, 5241 (1999).
[9] T. S. Majmudar and R. P. Behringer, Nature **435**, 1079 (2005).
[10] J. Brujic, S. Fedwards, I. Hopkinson, and H. Makse, Physica A **327**, 201 (2003).
[11] J. Zhou, S. Long, Q. Wang, and A. D. Dinsmore, Science **312**, 1631 (2006).
[12] G. Katgert and M. van Hecke, Europhys. Lett. **92**, 34002 (2010).
[13] C. S. O'Hern, L. E. Silbert, A. J. Liu, and S. R. Nagel, Phys. Rev. E **68**, 011306 (2003).
[14] E. Gardel *et al.*, Phil. Trans. R. Soc. A **367**, 5109 (2009).
[15] D. Weaire, J. D. Barry, and S. Hutzler, J. Phys.: Cond. Matt. **22**, 193101 (2010).
[16] G. Picard, A. Ajdari, F. Lequeux, and L. Bocquet, Eur. Phys. J. E **15**, 371 (2004).
[17] J. Goyon, A. Colin, G. Ovarlez, A. Ajdari, and L. Bocquet, Nature **454**, 84 (2008).
[18] L. Bocquet, A. Colin, and A. Ajdari, Phys. Rev. Lett. **103**, 036001 (2009).
[19] A. Kabla and G. Debregeas, Phys. Rev. Lett. **90**, 258303 (2003).
[20] E. Longhi, N. Easwar, and N. Menon, Phys. Rev. Lett. **89**, 045501 (2002).
[21] R. Shah *et al.*, Mater. Today **11**, 18 (2008).
[22] K. Desmond and S. V. Franklin, Phys. Rev. E **73**, 031306 (2006).
[23] I. Albert *et al.*, Phys. Rev. E **64**, 031307 (2001).
[24] D. W. Howell, R. P. Behringer, and C. T. Veje, Chaos **9**, 559 (1999).